Chemical Engineering Science 127 (2015) 95–105

Contents lists available at ScienceDirect

Chemical Engineering Science

journal homepage: www.elsevier.com/locate/ces

An investigation on the mechanics of homogeneous expansion in gas-fluidized beds

Oyebanjo Oke, Paola Lettieri, Luca Mazzei*

Department of Chemical Engineering, University College London, WC1E 7JE London, UK

HIGHLIGHTS

- We model the stable expansion in gas-fluidized beds of different diameters.
- We solve the model and analyze the results using the Richardson and Zaki equation.
- We study the role of enduring particle–particle contacts in uniform gas-fluidized beds.
- We study the role of wall friction in uniform gas-fluidized beds.
- We conduct fluidization/defluidization experiments to validate our theoretical results.

ARTICLE INFO

Article history:
Received 12 November 2014
Received in revised form
5 January 2015
Accepted 8 January 2015
Available online 17 January 2015

Keywords:
Fluidization
Homogeneous bed expansion
Cohesive powders
Interparticle forces
Enduring particle–particle contacts

ABSTRACT

The Richardson and Zaki (1954, Sedimentation and fluidization. *Trans. Inst. Chem. Eng.* 32, pp. 35–53.) equation has been used extensively to investigate the expansion profiles of homogeneous gas-fluidized beds. The experimental value of the parameter n appearing in the equation indicates how significantly interparticle forces affect the expansion of these beds, revealing the relative importance of these forces with respect to the fluid dynamic ones. In this work, we modeled the stable expansion of gas-fluidized beds of different diameter, accounting for enduring contacts among particles and wall effects. We solved the model numerically to obtain the bed expansion profiles, back-calculating from them the values of the parameter n. For all the cases considered, we observed that the values of n are higher than those obtained by purely fluid dynamic correlations, such as those advanced by Richardson and Zaki, and Rowe (1987, A convenient empirical equation for estimation of the Richardson and Zaki exponent. *Chem. Eng. Sci.* 42, pp. 2795.). This effect was more pronounced in beds of smaller diameter. To validate our model, we carried out fluidization and defluidization experiments, analyzing the results by means of the Richardson and Zaki equation. We obtained a reasonable agreement between numerical and experimental findings; this suggests that enduring contacts among particles, which are manifestations of cohesiveness, affect homogeneous bed expansion. This effect is amplified by wall friction.

1. Introduction

Gas-fluidized beds generally exhibit heterogeneous structure, with rising pockets of gas named *bubbles*; liquid-fluidized beds, conversely, usually maintain a smooth appearance, expanding progressively as the fluid flow rate is increased. These two types of fluidization behaviors are respectively termed *aggregative or bubbling* (for gas-fluidized beds) and *particulate or homogeneous* (for liquid-fluidized beds). Although gas-fluidized beds generally exhibit aggregative fluidization, small particles with low density fluidized by gas display an interval of smooth expansion when the flow rate of fluid exceeds the minimum fluidization value (Tsinontides and Jackson, 1993). Particles with this stable behavior are classified by Geldart (1973) as Group A powders.

The physical origin of the stable behavior of Group A powders has been studied by several researchers. Some ascribed the stability of uniform suspensions to the effect of interparticle forces, while others sought for a purely fluid dynamic explanation. Jackson (1963) carried out a fluid dynamic stability analysis, but was unable to predict the stable behavior of gas-fluidized beds of fine materials. Also Garg and Pritchett (1975) investigated the dynamics of gas-fluidized beds theoretically, reporting that stability can be predicted by adding to the particle linear momentum balance equation a fluid dynamic force proportional to the spatial

* Corresponding author.
E-mail address: l.mazzei@ucl.ac.uk (L. Mazzei).

http://dx.doi.org/10.1016/j.ces.2015.01.020

gradient of the fluid volume fraction. Foscolo and Gibilaro (1984) derived a stability criterion based on fluid dynamic arguments, resorting to the stability theory of Wallis (1969), to show that stability depends on the relative magnitude of the kinematic and dynamic waves that propagate in the bed (Mazzei et al., 2006; Mazzei, 2008). Similarly to Garg and Pritchett (1975), they reported that the force acting on the particles (in particular the drag component), present in the particle linear momentum balance equation, should contain an additional term proportional to the spatial gradient of the bed void fraction. Batchelor (1988) held a view which is similar in part to that of Foscolo and Gibilaro (1984). He proposed a predictive criterion for stability based on fluid dynamic considerations. But he did not support the idea that stability is a result of the dependence of the drag force on the void fraction gradient, as Foscolo and Gibilaro (1984) maintained; he showed instead that stability can arise from random fluctuations in the particle velocity.

Reitema (1973) and Mutsers and Reitema (1977), conversely, adopted the stability criterion of Wallis (1969) to show that the stable behavior observed in Group A powders may be attributed to the cohesive forces among particles. Their experiments show that when a uniform gas-fluidized bed is tilted over a horizontal axis, it remains stable until a critical tilting angle is reached, and at this angle the bed surface suddenly shears off. This observation demonstrates that uniform gas-fluidized beds maintain a mechanical structure that is caused by sustained contacts among particles. Mutsers and Reitema (1977) further argued that, if the stability of gas-fluidized beds is due to fluid dynamic forces, the voidage at minimum bubbling should depend on the ratio g/μ_g^2; conversely, if the stability is due to a network of interparticle contacts, it should depend on g/μ_g. Their experimental results showed that the latter holds, validating their claim that stability results from the action of interparticle forces.

Tsinontides and Jackson (1993) also investigated the mechanism of stabilization of gas-fluidized particles. They carried out fluidization and defluidization experiments of fine powders about complete cycles, from zero gas flow rate up to flow rates where bubbles start appearing in the bed and then back to zero. They measured the bed depth and pressure drop at each stage, determining the solid volume fraction profiles by employing a high-resolution gamma-ray densitometer. Their results revealed the presence of yield stress throughout the range of stable behavior. They thus concluded that the stability of gas-fluidized particles is due to the presence of particle–particle contact forces.

While attempting to explain the physical origin of stability in gas-fluidized beds, Fortes et al. (1998) used a theoretical approach to show that the stability of these systems has two distinct origins: one that is fluid dynamic, arising from the interactions between the solid and fluid phases, and one that is not, arising from interparticle forces. They proposed a mechanistic description for the latter, regarded as a stabilizing agent of fluidization, showing that clustering and particle dispersion in suspensions result from the competition between interparticle and fluid dynamic forces.

While the arguments among researchers on the physical origin of the stable behavior of gas-fluidized beds continue, some pertinent questions about these systems arise. Do homogeneous gas-fluidized beds consist of particles that float freely without interacting? Furthermore, if we deny the existence of particle–particle contact forces in these beds, how do we explain with fluid dynamic considerations alone the presence of particle interactions that often result in the formation of clusters? Valverde et al. (2003b) sought to answer these probing questions in their experimental work on the dynamics of gas-fluidized beds. They reported that the interval of stability observed in gas-fluidized Group A particles has two regimes, one with *'solid-like'* and another with *'fluid-like'* behavior. Castellanos (2005) examined the distinctive features of these regimes in the fluidization–defluidization experiments of xerographic toner particles. He reported that the solid-like regime is characterized by the existence of a network of permanent particle–particle contacts that stabilizes the bed against small perturbations. In this regime, the bed behaves like a weak solid with non-vanishing compressive and tensile yield stress. In the fluid-like regime, conversely, particle contacts are absent and the bed behaves like a low-viscosity liquid whose upper surface remains horizontal when tilted. These observations strengthen the idea that the stability of gas-fluidized beds may have two distinct origins: one purely fluid dynamic and one arising from particle contact forces.

In this work, we attempt to provide further insight into the stable behavior of homogeneous gas-fluidized beds. We believe that the effect of cohesiveness in these systems is reflected by the presence of enduring contacts among particles. Such contacts are characteristic of homogeneous gas-fluidized beds in the solid-like regime; therefore, we focused our analysis primarily on this regime. We carried out fluidization and defluidization experiments, analyzing the results by means of the Richardson and Zaki (1954) equation. We solved the one-dimensional linear momentum balance equations of Jackson (2000) for the fluid and solid phases, accounting for enduring contacts among particles, relating the numerical predictions of the model to our experimental findings. Now, to begin, we review the Richardson and Zaki equation, discussing on its ability to predict the expansion profiles of gas-fluidized beds.

2. Richardson & Zaki equation and homogeneous expansion of gas-fluidized powders

Richardson and Zaki (1954) advanced an empirical relationship between the sedimentation velocity u of monodisperse particles in a liquid and the void fraction ε of the dispersion. The equation reads

$$u = u_t \varepsilon^n \tag{1}$$

where n is an empirical parameter which depends on the free fall particle Reynolds number Re_t, and u_t is the unhindered terminal settling velocity of the particles. Several correlations have been proposed for determining the value of n. In particular, we report the empirical relationship proposed by Rowe (1987), which we used in this work

$$n(Re_t) = \frac{A + B \times 0.175 Re_t^{3/4}}{1 + 0.175 Re_t^{3/4}} \tag{2}$$

Here A and B are the values ascribed to n in the limits of viscous and inertial regimes, respectively. Richardson and Zaki (1954) take A and B to be equal to 4.65 and 2.39, respectively; Rowe (1987) employs the values of 4.70 and 2.35, while Khan and Richardson (1989) and Gibiliaro (2001) use 4.80 and 2.40, respectively. The unhindered terminal settling velocity u_t, on the other hand, can be obtained in the creeping flow regime using the well-known Stokes equation

$$u_t = \frac{(\rho_p - \rho_f) g d_p^2}{18 \mu_f} \tag{3}$$

Here μ_f and ρ_f are the viscosity and density of the fluid, respectively, d_p and ρ_p are the particle diameter and density, respectively, and g is the gravitational acceleration.

The Richardson and Zaki (1954) equation and the correlations proposed for estimating the exponent n are found to hold for liquid-fluidized systems, where they are very accurate in providing an excellent account of the expansion profiles of such systems. But questions were raised regarding the applicability of this correlation

to gas-fluidized systems. While trying to answer these questions, Godard and Richardson (1968) conducted several experiments on powders fluidized by air and characterized by extremely narrow size distributions. They found that the relationship between the superficial fluid velocity and the void fraction could be expressed in the Richardson and Zaki form, given in Eq. (1); however, the values of the exponent n for all the powders tested were found to be greater than those predicted by Eq. (2). They also found that the values of the parameter u_t determined by extrapolating the logarithmic void fraction-velocity plots were greater than the terminal velocity of the particles. To emphasize this, we shall denote these experimental values as n^* and u_t^*. The latter, as said, differ from the fluid dynamic values of n and u_t observed in liquid-fluidized beds and predicted by Eqs. (2) and (3), respectively.

Massimilla et al. (1972) and Donsi and Massimilla (1973) investigated the homogeneous expansion of fine particles fluidized by gas and report that the value of the exponent n^* is between 5.4 and 7.0. Again, these values are outside the range predicted by the empirical correlations reported above for liquid-fluidized beds.

Lettieri et al. (2002) studied the homogeneous bed expansion of FCC catalysts fluidized by gases at high temperatures. They employed the Richardson and Zaki equation to describe the homogeneous expansion of these particles, estimating the values of the parameters in the equation. These values were compared with those of n and u_t predicted by Eqs. (2) and (3), respectively; for all the FCC catalysts considered, they found that the former (that is, n^* and u_t^*) were much higher than the latter (that is, n and u_t). They attributed this to the formation of clusters in the bed, which are caused by the presence of interparticle forces.

In the same vein, Geldart and Wong (1984, 1985) investigated the bed expansion characteristics of Group A powders. They fluidized different materials with different gases and found the values of n^* between 4 and 60, showing that materials with higher cohesiveness have greater values of the exponent. Moreover, they observed that in non-cohesive systems, the value of the terminal velocity given by the Stokes equation is very close to that extrapolated from the logarithmic plot of the Richardson and Zaki equation, whereas for cohesive systems it is greater.

All the foregoing experimental evidence, and much more not reported here, allows us to conclude that the Richardson and Zaki equation is capable of describing the bed expansion of gas-fluidized particles, but the values of the equation parameters are greater than those required for liquid-fluidized systems (in general, fluidized systems in which fluid dynamic forces dominate over interparticle forces). Researchers have presented compelling experimental evidence to show that the greater values obtained for the parameters are indications of the presence of interparticle forces. These observations appear to support the idea that these forces play a crucial role in the stabilization of gas-fluidized fine powders.

We should note that the expansion of non-cohesive homogeneous powders depends only on the drag force exerted by the fluid on the particles, in addition to the effective weight of the latter; as a consequence, the values of n and u_t (which refer to liquid-fluidized beds, in which interparticle forces are negligible compared to their fluid dynamic counterpart) are directly related to the drag force magnitude. Conversely, the expansion of cohesive powders depends not only on the fluid dynamic forces just mentioned, but also on the forces that the particles exert on one another; accordingly, the values of n^* and u_t^* (which refer to gas-fluidized beds, in which interparticle forces are often as important as their fluid dynamic counterpart) lump together the effects of both forces and are not directly related only to the drag force magnitude. This observation is important when one intends to model the drag force.

In this work, our goal is to investigate the homogeneous regime in gas-fluidized beds, intending to show that the stress transmitted through sustained contacts among particles plays a role in the bed homogeneous behavior and is responsible for the higher values of n^* and u_t^* observed experimentally for fine particles. This will offer further insight into the dynamics of stable expansion in fluidized beds. The conventional idea is that these beds consist of particles freely suspended in the fluid with no form of particle–particle interactions. Nevertheless, as we shall see, homogeneous fluidized beds are not necessarily systems with uniform solid volume fraction which are entirely supported by the fluid: this is only observed in beds that are in the fluid-like regime. More often, homogeneous beds are in the solid-like regime, and so are only partly fluidized, presenting a solid volume fraction gradient along the vertical bed axis. One often uses the Richardson and Zaki (1954) equation to describe the bed expansion of any kind of homogeneous bed, although the equation was derived merely for beds in the fluid-like regime, in which interparticle forces are absent or negligible. This aspect has to be investigated in more detail. This is what we intend to do. To this end, we employed a theoretical model to analyze the expansion of gas-fluidized powders, taking into consideration enduring particle–particle contacts. We used the model to determine the axial void fraction profiles through the bed at different superficial gas velocities. By plotting the mean void fraction against the superficial gas velocity in the Richardson and Zaki form, we computed the values of the parameters n and u_t which appear in the correlation. We then conducted fluidization and defluidization experiments to validate our theoretical results. Before presenting the model, we briefly describe the processes of fluidization and defluidization, on which the remaining part of this work focuses.

3. The processes of fluidization and defluidization of fine particles

In describing these processes, we find it more convenient to examine defluidization first. Consider a fluid bed of small, light particles, such as those belonging to Group A of the Geldart (1973) classification. We assume that the bed is homogeneous and in the *fluid-like* regime, so that *no enduring contacts are present* among the particles. These, in consequence, are fully supported by the fluid. Being the bed homogeneous, the volume fraction of solid, denoted as ϕ, is uniform throughout it. If we slightly decrease the fluid flow rate, the bed contracts, remaining uniform and in the fluid-like regime, until ϕ attains the value needed by the drag force to balance the effective weight of the bed. If we continue to decrease the fluid flow rate, the volume fraction of solid will eventually reach a value $\phi_{\min}$ at which the granular material is able to resist compression. When the bed reaches this compaction, it enters the *solid-like* regime, in which *particles do form enduring contacts* and the bed starts behaving like a weak solid. The more ϕ exceeds the value $\phi_{\min}$ (that is, the more compact the bed), the larger the stress needed to cause compressive yield (that is, further bed compaction). We assume that the compressive yield stress tends to infinity at some value $\phi_{\max}$; when the bed reaches this compaction, it cannot compact further, no matter how large the compressive stress to which it is subjected becomes. Hence, with Tsinontides and Jackson (1993), we can model the compressive yield stress using the following constitutive equation

$$\sigma_c(\phi) = c\frac{(\phi-\phi_{\min})^a}{(\phi_{\max}-\phi)^b} \quad \phi_{\min}<\phi<\phi_{\max},$$
$$= 0 \qquad \phi<\phi_{\min} \tag{4}$$

where a, b and c are positive constants which must be determined experimentally. As said, $\phi_{\min}$ denotes the lowest solid volume

fraction at which the assembly of particles is capable of supporting stress through a structure of enduring contacts, whilst ϕ_{max} denotes the highest solid volume fraction that one can obtain in a defluidization process without resorting to mechanical means. The interval between ϕ_{max} and ϕ_{min} is largely determined by the *cohesiveness* of the material. For large, smooth, non-cohesive particles, such as those belonging to Groups B and D of the Geldart (1973) classification, ϕ_{max} and ϕ_{min} are very close; this is because particles are brought to random close packing under very small compressive stress, insofar as they are unable to form a network of enduring contacts. For small, rough, cohesive particles, which are able to form such a network, the interval between ϕ_{max} and ϕ_{min} is instead much larger. These groups of particles are able to form extended structures which can resist compressive stress over a broader range of particle concentration. This might explain why, during fluidization, they can expand homogeneously over a wide range of superficial gas velocity before transiting to the bubbling fluidization regime. In this work, we focus on this second group of particles.

When the bed enters the solid-like regime, its structure is uniform – the solid volume fraction being equal to ϕ_{min} everywhere. In this condition, the bed is still fully supported by the fluid. But when the fluid flow rate is decreased further, the bed compacts non-uniformly, the mean bulk density increasing progressively from the top of the bed to its bottom: *a solid volume fraction profile develops along the vertical bed axis*. In particular, if we assume that the bed is in a condition of incipient yield everywhere, in each location the solid volume fraction takes the value required by the compressive yield stress to equate the compressive stress present at that location. The bed is only *partially fluidized*, being partly supported by the distributor plate and partly by the frictional forces acting between the walls of the vessel and the particles. And even if the bed may look homogeneous to the naked eye, it is not. When the fluid flow rate vanishes, the bed is completely defluidized and fully supported by the distributor plate and the vessel walls; also in this case, the bed is inhomogeneous, the solid volume fraction increasing towards the bed bottom.

Consider now the bed of granular material that is resting on the distributor plate. If an upward flow of gas is established, the bed structure, and in particular the solid volume fraction profile along the vertical axis of the bed, initially remains unchanged, the pressure drop through the bed rises, and the particles become partly supported by the drag force exerted on them by the fluid. At a sufficiently large flow rate, the bed weight is entirely supported by the drag force, but in general the bed retains its structure, without dilating (in other words, it does not fluidize). A further increase in gas flow rate generates tensile stress within the granular material. When the latter exceeds the tensile yield stress which the material may sustain, the bed breaks and fluidization begins. When this happens, the pressure drop, and hence the drag force, is equal to the sum of the weight of the bed and the tensile yield stress which must be exceeded before the bed dilates (Tsinontides and Jackson, 1993; Watson et al., 2001).

The condition for the bed to dilate, according to Tsinontides and Jackson (1993), is first met at the contact surface between the bed and the distributor plate; thus, the fluidization process commences by the fracture of the bed at its lowest point. When this happens, the stress at the bottom and top of the bed vanishes and the bed accelerates upwards. The acceleration is caused by the imbalance between the bed weight and the drag force; the latter, as said, is greater than the former when the bed detaches from the distributor plate. As the bed travels upwards, its bottom part, which is a free surface, gradually erodes, generating a rain of particles behind it. These particles recompact to form a new, more dilute bed. While the fluid flow rate is kept constant, the original packed bed continues to travel upward, gradually becoming shorter in length as its lower region progressively disappears, until it is entirely replaced by the new bed (for low fluidization velocities, near minimum fluidization, the behavior complicates slightly; refer to Tsinontides and Jackson (1993)). This dynamic process is complex, and since we also lack an exact understanding of the mechanics of erosion, predicting how the newly-formed bed is structured (particularly, how the solid volume fraction varies along the bed axis) is not possible. We do not expect the bed to be at incipient yield conditions, but nothing can guarantee that it is fully supported by the fluid (and therefore fully fluidized).

We conclude this section by pointing out that the values of ϕ_{max} and ϕ_{mf} (the solid volume fraction at minimum fluidization) are expected to be very close, because the bed does not expand while it is fixed. If a powder does not enter the fluid-like regime during homogeneous fluidization, then ϕ_{min} and ϕ_{mb} (the solid volume fraction at minimum bubbling) are expected to be identical; conversely, if a powder enters the fluid-like regime, ϕ_{min} is expected to be larger than ϕ_{mb}.

4. Theoretical analysis

The theoretical analysis is based on the one-dimensional model derived by Jackson (2000). We report the main equations of the model, referring to the literature for details. The linear momentum balance equation for the fluid phase in the regime of stable bed expansion reads

$$\frac{dp}{dz}=\frac{\phi(\rho_p-\rho_f)g}{(1-\phi)^n}\frac{u}{u_t}+\rho_f g \tag{5}$$

where p is the fluid pressure and z is the vertical coordinate *measured downwards from the upper surface of the bed*. Notice that the Richardson and Zaki parameters featuring in this equation are the fluid dynamic ones (that is, n and u_t) because the drag force is entirely unrelated to particle–particle interaction forces. If we used the experimental values n^* and u_t^*, we would no longer be modeling the drag force; we would be modeling an *effective force* combining the drag and interparticle forces. This was mentioned in Section 2. Accordingly, to calculate the values of n and u_t in Eq. (5), we employed Eqs. (2) and (3), which are purely fluid dynamical and unrelated to particle–particle contacts.

The linear momentum balance equation for the solid phase in the regime of stable bed expansion, which, as for the fluid, reduces to a force balance, reads

$$\frac{d\sigma}{dz}\pm\frac{4}{D}\mu j\sigma=\phi(\rho_p-\rho_f)g\left[1-\frac{1}{(1-\phi)^n}\frac{u}{u_t}\right] \tag{6}$$

where σ is the zz-component of the stress, D is the bed diameter, μ is the coefficient of wall friction, j is the Janssen coefficient, while u is the superficial velocity of the fluid. The first term on the left-hand side relates to the forces transmitted via particle–particle contacts. In this work, we aim to investigate how their presence influences the behavior of the bed, in particular its homogeneous expansion. The second term represents the frictional force exerted on the particle assembly by the walls of the vessel containing the fluid bed; the positive sign applies to the defluidization process, in which the bed slowly consolidates, while the negative sign applies to the fluidization process. The term on the right-hand side combines the gravitational force acting on the particles and the fluid–particle interaction force.

In Eq. (6) there are two unknown functions: $\sigma(z)$ and $\phi(z)$. To find the solid volume fraction profile $\phi(z)$ in the bed, we need to express the normal stress σ as a function of ϕ and then substitute this expression in the linear momentum balance equation. During *defluidization*, the variables σ and ϕ are related, if we assume that

the bed is in conditions of incipient yield everywhere; thus, following Tsinontides and Jackson (1993), we can employ Eq. (4). In Section 5, we will report how we obtained the values of the constants in the equation. Consequently, for a defluidization process, we can write

$$\frac{d\phi}{dz}=\frac{d\sigma}{dz}\left[\frac{d\sigma}{d\phi}\right]^{-1}=\left\{(\rho_p-\rho_f)\phi g\left[1-\frac{u}{u_t}\frac{1}{(1-\phi)^n}\right]-\frac{4}{D}\mu j\sigma\right\}\left[\frac{d\sigma}{d\phi}\right]^{-1} \quad (7)$$

where the derivative of $\sigma(\phi)$ can be calculated by means of Eq. (4). The values of j and μ are related to the angle of internal friction φ as follows:

$$j=\frac{(1-\sin\varphi)}{(1+\sin\varphi)} \quad ; \quad \mu=\frac{k_c}{\sigma}+\tan\varphi \quad (8)$$

where k_c is the particle–wall cohesion coefficient, which we assume to be negligibly small since no strong cohesion is present between the particles and the steel walls of the vessel (Mabrouk et al., 2008). Note that, as mentioned, the angle of internal friction is employed also to model the particle–wall coefficient μ, as done in several other works in the literature (see, for instance, Mabrouk et al. (2008); Cagnoli and Manga (2004); Hartl and Ooi (2011)).

To calculate the solid volume fraction profile in the bed at each operating condition, we integrate Eq. (7), using the following boundary condition

$$z=0, \quad \phi=\phi_{\min} \quad (9)$$

This condition is given at the lower limit of the integration domain, which coincides with the top surface of the bed. The upper limit of the integration domain, which coincides with the bottom surface of the bed, located at $z=H$, where H denotes the bed height at the given operating condition, is unknown at the start of the numerical integration. To determine it, we start integrating Eq. (7) from the top of the bed, terminating the integration at the value of H which satisfies the following condition

$$\rho_p\int_0^H\phi(z)dz=m \quad (10)$$

where m is the particle mass loading, that is, the mass of particles per unit cross-sectional area. Thus, by imposing the condition reported in Eq. (10) on the solution of Eq. (7), we can determine the solid volume fraction profile $\phi(z)$ and the bed height H for a given superficial fluid velocity. Knowing $\phi(z)$ allows us to integrate Eq. (5) to obtain the fluid pressure profile at different values of u.

In the *fluidization* process, if we assume that the tensile yield stress of the powder is vanishingly small, we can argue that, as the velocity is gradually increased from zero, σ at the bottom of the bed decreases to finally vanish when the minimum fluidization velocity u_m is reached. Following this argument, we can determine the value of u_m as follows. During fluidization, Eq. (6) reads

$$\frac{d\sigma}{dz}-\frac{4}{D}\mu j\sigma=(\rho_p-\rho_f)\phi g\left[1-\frac{u}{u_t}\frac{1}{(1-\phi)^n}\right] \quad (11)$$

In this case, σ and ϕ are no longer functionally related; so, Eq. (11) cannot be solved to obtain $\phi(z)$ at each superficial gas velocity, as we did during the defluidization process. For fluidization velocities lower than the minimum fluidization velocity, this does not present a problem, because the bed retains the structure acquired during the defluidization process, and therefore the solid volume fraction profile $\phi(z)$ is known, being equal to that obtained during defluidization for a zero fluid velocity. This allows us to solve Eq. (11) to determine the stress profile $\sigma(z)$. Once this is known, we can find the minimum fluidization velocity u_m, because, as reported in Section 3, we know that at minimum fluidization σ vanishes at the top and bottom of the bed. The velocity is given by

$$\frac{u_m}{u_t}=\left(\int_0^H\phi e^{-pz}dz\right)\left(\int_0^H\frac{\phi}{(1-\phi)^n}e^{-pz}dz\right)^{-1} \quad (12)$$

where $p\equiv 4\mu j/D$. This equation allows calculating the value of the minimum fluidization velocity given the axial profile $\phi(z)$. The latter, as said, is the solid volume fraction profile obtained in the defluidization process when the gas flow rate is zero (that is, the bed is fully defluidized).

5. Experimental

We investigated two types of powders: Powder 1 (Alumina) and Powder 2 (Ballotini). Their properties are reported in Table 1. For each powder we performed two sets of experiments: first, fluidization and defluidization experiments, which allowed us to determine the pressure drop and bed height profiles in the bed; second, experiments aimed to determine the compressive yield stress σ of the powder, which allowed us to obtain the values of the parameters appearing in Eq. (4).

5.1. Fluidization and defluidization experiments

We carried out fluidization and defluidization experiments in three different tubes, made of stainless steel, with nominal internal diameters of 10 cm, 5 cm and 2.5 cm, and height of 1 m. We chose stainless steel as vessel material to minimize electrostatic effects. The latter usually arise as a result of continuous contact and separation between the particles and the vessel walls. Electrostatic effects create serious problems in fluidized beds, making particles adhere to the wall and in some cases generating channeling. One method suggested by Katz and Sears (1969) to minimize these effects is to increase the humidity of the fluidizing gas. We did not resort to this method, because it would increase the cohesiveness of the particles, making it impossible to distinguish between the effects of air humidity and those (that continue to be) present also in dry conditions. In any case, the electrostatic effects were reduced significantly with the use of stainless steel as vessel material. The gas distributor, made of a 5 mm-thick sintered mesh with pore size of 20 μm, was mounted between the tubes and the windbox (whose diameter, in each case, was equal to that of the tube). We used dry air, from compressed air cylinders, as fluidizing medium, passing it through a pressure regulator to minimize flow fluctuations. We measured the gas flow rates by means of flow meters and the pressure drops across the bed by means of a digital manometer.

To visualize the bed, we used a pulsed x-ray system consisting of an x-ray generator, an x-ray tube and an image intensifier, respectively labeled 1, 2 and 3 in Fig. 1. The x-ray tube and the image intensifier are mounted on a twin column suspension unit that allows them to be moved vertically or horizontally across the room. The horizontal movement allows us to adjust the distance between the x-ray tube and the image intensifier, while the vertical movement allows us to visualize different heights in the fluidized bed. Each column can be moved vertically independently

Table 1
Physical properties of powders 1 and 2.

	Powder 1	Powder 2
Mean particle diameter (μm)	53	66
Particle density (kg/m^3)	1730	2500
Angle of internal friction, φ	40°	13°
Minimum fluidization velocity (cm/s)	0.113	0.633
Minimum bubbling velocity (cm/s)	0.301	0.971

Fig. 1. Experimental set-up showing the x-ray equipment for visualizing the fluidized bed. (1) x-ray generator, (2) x-ray tube, (3) image intensifier.

or as a synchronized pair. The x-rays are produced from a high-voltage source ranging from 40 to 150 kV and frequencies up to 72 Hz, pulsed at 25 fps. The x-ray pulses, synchronized with an image capturing device, pass through the fluid bed. The absorption of the x-rays by the latter is proportional to the nature and quantity of the material along its path. The x-ray beam that emerges from the fluid bed is amplified by the image intensifier by converting the x-ray absorption pattern to an image of sufficient brightness and contrast. These are then recorded by a video camera. The images from the camera are sent by fiber optics to a dual processor industrial PC that has the capacity to store real-time image sequences of high quality.

To start the experiments, we placed a known mass of particles in the tube. We aerated the bed at low flow rate for about 30 min to ensure that the particles were moisture-free. We then increased the flow rate, allowing the bed to bubble gently for a period of time. After, we decreased the air flow in small intervals until the bed was entirely defluidized. At each step, we let the bed equilibrate, subsequently measuring the bed height and pressure drop. After completing the defluidization process, we increased the air flow rate in small increments, measuring at each step the bed height and the pressure drop through the bed until the latter entered the bubbling regime. The pressure drop curves, for different vessel diameters, are reported in Fig. 2 for both fluidization and defluidization processes; the figure refers to Powder 1, but analogous trends are observed for Powder 2. The profiles obtained numerically are also shown; we will discuss them later on in Section 6.

5.2. Determination of the powder compressive yield stress

To determine the compressive yield stress of the powders investigated, we adopted a procedure proposed by Valverde et al. (1998). We placed a known mass of particles *in the tube with diameter of* 10 cm. We allowed the bed to bubble gently for a while, and then we slowly reduced the gas flow rate until it became entirely defluidized. We finally measured the bed height. We then added a known mass of particles to the bed, letting the latter bubble gently for a while, then, we slowly defluidized it, recording its resting height. By repeating this procedure, we

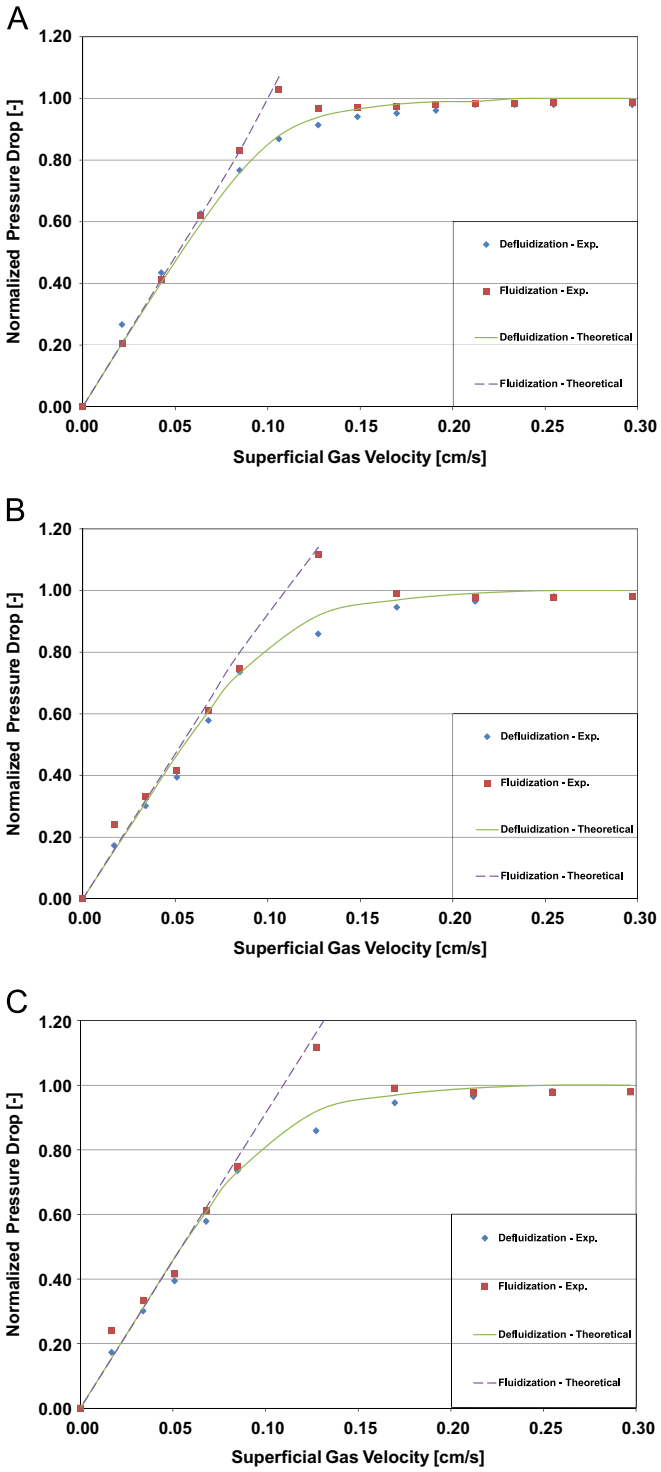

Fig. 2. Normalized pressure drop, defined as $\Delta P/(mg)$, against superficial gas velocity for Powder 1. ΔP is the pressure drop, m is the mass of the powder per unit cross-sectional area of the tube and g is the gravitational acceleration. Figures A, B and C refer to tube diameters of 10 cm, 5 cm and 2.5 cm, respectively.

obtained the bed height H as a function of the mass loading m. We then calculated the mean solid volume fraction $\overline{\phi}(H)$ for each value of H using this relation

$$\overline{\phi}(H) = \frac{m}{\rho_p g H} \tag{13}$$

The variation with H of the experimental values obtained for $\overline{\phi}$, along with a curve fit, is shown in Fig. 3 for Powders 1 and 2. We

see that $\overline{\phi}$ increases rapidly when the bed is shallow, remaining approximately constant when it becomes sufficiently deep. This constant value gives a rough estimate of ϕ_{max}. We now use these figures to determine the compressive yield stress curves for the two powders.

The increase in $\overline{\phi}$ as the bed height increases is caused by an increase in compressive stress, owing to the weight of the particles; this makes the latter rearrange into a more compact ensemble in the lower parts of the bed. Assuming that wall friction plays a negligible role – this is why to carry out these measurements we used the vessel of largest diameter – we can calculate the compressive yield stress *at the bottom of the bed* using the following relation:

$$\sigma(H) = \rho_p \overline{\phi}(H) g H \tag{14}$$

If we now succeed in determining the corresponding values of $\phi(H)$, that is, of the solid volume fractions *at the bottom of the bed* for the various bed heights considered, combining the functions $\sigma(H)$ and $\phi(H)$ we can obtain the compressive yield stress locus $\sigma(\phi)$. Our task is thus finding a way to obtain the values $\phi(H)$. These differ from those of $\overline{\phi}(H)$: the former are the local values of the solid volume fraction at the bottom of the bed, whereas the latter are the mean values of the solid volume fraction, averaged over the entire bed. To derive an expression for $\phi(H)$, we proceed as follows. We begin by writing

$$\int_0^H \phi(z)dz = \overline{\phi}(H)H \tag{15}$$

Differentiating both sides with respect to H, we obtain

$$\phi(H) = \overline{\phi}(H) + H\frac{d\overline{\phi}}{dH} \tag{16}$$

We can now use the experimental curve $\overline{\phi}(H)$ reported in Fig. 3 and Eq. (16) to evaluate $\phi(H)$ and use Eq. (14) to evaluate $\sigma(H)$. Fig. 4 reports the curves $\sigma(\phi)$ for Powders 1 and 2 obtained with this method. The figure shows that the stress needed to cause compressive yield is small at low values of ϕ, but, as the latter increases, σ rises slowly at first and then rapidly. To obtain the values of the parameters that appear in Eq. (4), we fitted the equation to the experimental curves in Fig. 4; the results are reported in Table 2, along with other properties of the powders.

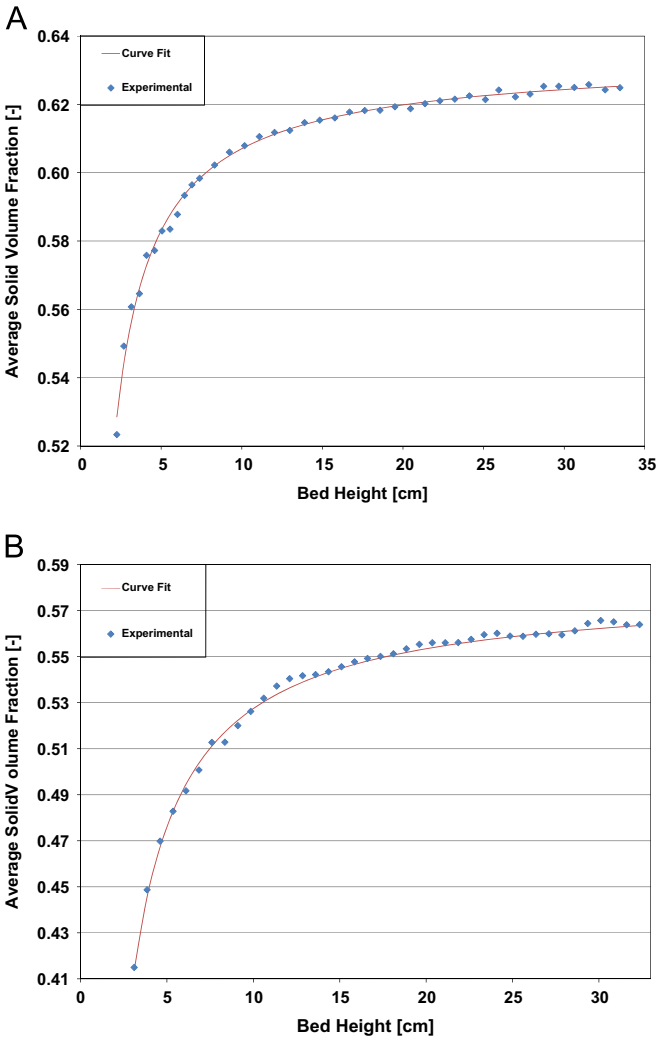

Fig. 3. Average solid volume fraction against bed height obtained experimentally. Figures A and B refer to Powders 1 and 2, respectively.

6. Results and discussion

As said, Fig. 2 refers to Powder 1 and reports the plots, obtained through fluidization and defluidization experiments, of the pressure drop, normalized with respect to the bed weight per unit cross-sectional area of the tube, against the superficial gas velocity; cases A, B and C refer to tube diameters of 10 cm, 5 cm and 2.5 cm, respectively. Similar profiles, not shown, were obtained for Powder 2. In Fig. 2, during the fluidization process, the normalized pressure drop rises linearly until the velocity reaches the minimum fluidization value. At this point, the normalized pressure drop increases above unity, revealing that the pressure drop through the bed exceeds the effective bed weight. This is observed for all the tube diameters investigated. There is a noticeable increase in the pressure drop overshoot as the bed diameter decreases; we attribute this to wall effects, which become more pronounced as the tube diameter becomes smaller. Similar pressure drop overshoots have been reported by several authors (see, for instance, Tsinontides and Jackson (1993); Valverde et al. (1998); Srivastava and Sundaresan (2002)). We observe that the normalized pressure drop at fluidization velocities beyond the point of initial expansion is less than unity; this means that the pressure drop does not support the full weight of the bed, and that in the latter compressive stress is at work. This is contrary to what one would expect in ideal fluid beds, where the pressure drop exactly balances the effective weight of the particles, the solid being unable to transmit stress. Although the bed expands, it is not fully fluidized, being in the solid-like regime over the entire interval of stable expansion, before transiting to the bubbling regime at a superficial gas velocity of about 0.30 cm/s. This is observed, even more emphatically, during the defluidization process, starting from velocities close to the minimum bubbling velocity down to the point of minimum fluidization. Judging from the pressure drop curves, therefore, the bed never enters the fluid-like regime, even if eventually (that is, near the bubbling point) it approaches it very closely: when the superficial fluid velocity approaches the minimum bubbling velocity, in particular for fluid velocities greater than 0.24 cm/s, the normalized pressure drop becomes equal to 0.98 and the compressive yield stress almost vanishes. The fact that the bed does not appear to enter the fluid-like regime immediately before the onset of bubbling is not the crucial point; *for fluid velocities larger than* 0.24 cm/s, the normalized pressure drop is so close to unity that no clear-cut conclusions can be drawn. A slight underestimation of the pressure drop owing to experimental error may be present (although we are unaware of this); if so, the normalized pressure drop may *eventually* become unity, making us conclude that the bed does *eventually* enter the fluid-like regime. The important point, conversely, is that over

most of the interval of stable expansion the bed is in the solid-like regime.

The value of the solid volume fraction at minimum bubbling ϕ_{mb} reported in Table 2 is slightly lower than that of ϕ_{min}, implying that between these two solid volume fractions – *that is, for superficial fluid velocities larger than* 0.24 cm/s – the bed is in the fluid-like regime. The considerations reported above, in the previous paragraph, explain this contradiction. Also, because the difference between ϕ_{mb} and ϕ_{min} is not considerable, similar considerations to those made for the pressure drop apply here. Finally, we would like to point out that, as one can see from Table 2, for each powder the value of ϕ_{mb} does not depend on the vessel diameter (it is a property of the powder alone). This can be explained as follows. When the bed starts bubbling, the powder is either in the solid-like regime, but in this case, as Fig. 2 shows, *very near the threshold of fluid-like regime*, or in the fluid-like regime. This aspect has just been discussed. In the former case the compressive stress and in turn the friction force at the wall are negligibly small, while in the second case they are zero. So, in both cases at the bubbling point the wall plays a negligible role, in agreement with what is observed experimentally.

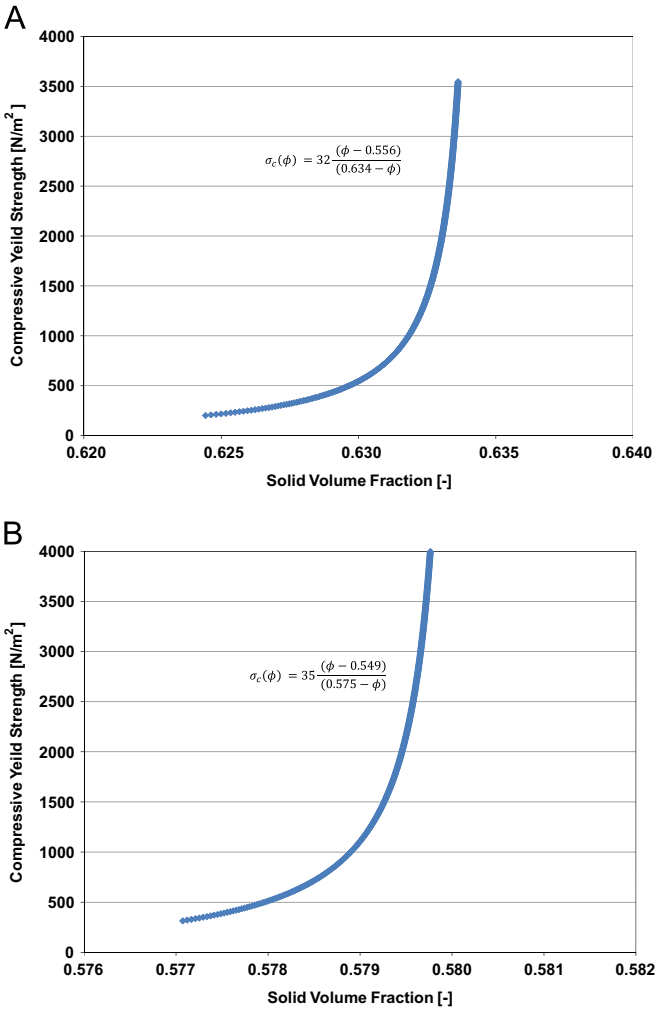

Fig. 4. Compressive yield stress σ against solid volume fraction ϕ obtained experimentally. Figures A and B refer to Powders 1 and 2, respectively.

The behavior just described is typical of Group A powders and has been reported often in the literature (refer, for instance, to Tsinontides and Jackson (1993); Jackson (2000); Srivastava and Sundaresan (2002); Loezos et al. (2002)). For more cohesive powders, such as those belonging to the Group C of the Geldart classification (treated in such a way that fluidization does occur), stable expansion is unambiguously present in both solid-like and fluid-like regimes, the latter, in particular, is clearly observed over a wide range of superficial gas velocities (Valverde et al., 2003a).

Fig. 2 reports also the theoretical fluidization and defluidization curves. The fluidization curves extend up to the superficial gas velocity at which the structure of the bed, acquired during defluidization, breaks down and fluidization begins. To continue these curves to higher superficial gas velocity values, we would have to assume something about the structure of the fluidized bed; as a consequence, we preferred to stop the fluidization curves at the end of the initial linear branch. The minimum fluidization velocities predicted theoretically, with the method described in Section 4, and those obtained experimentally, from the pressure drop curves referring to the fluidization and defluidization processes, are reported in Table 3.

For both fluidization and defluidization processes, the theoretical pressure drop curves reported in Fig. 2 match well the experimental ones, except in one respect. The theoretical curves during defluidization approach a value of unity when the gas velocity exceeds 0.24 cm/s; the model, therefore, predicts that between this velocity and the minimum bubbling velocity the bed finds itself in the fluid-like regime (this is also observed in Fig. 5A). This is consistent with the value of ϕ_{min} implemented in the model, which the suspension reaches at a gas velocity of 0.24 cm/s. For larger velocities, the model correctly predicts that particle contacts are no longer present and that the bed is spatially uniform.

6.1. Solid volume fraction profiles

By integrating Eq. (7) numerically, using for the parameters the values reported in Table 2, we determined the solid volume fraction profiles in the bed at various superficial gas velocities u during defluidization. Fig. 5 reports the solid volume fraction vertical profiles for Powders 1 and 2 at different superficial gas velocities. At each velocity, the volume fraction varies significantly

Table 2
Simulation parameters.

		Powder 1	Powder 2
Terminal velocity (m/s)	u_t	0.10	0.25
Richardson and Zaki exponent	n	4.60	4.30
Coefficient of wall friction	μ	0.80	0.27
Solid volume fraction beyond which enduring particle contacts vanish	ϕ_{min}	0.556	0.549
Maximum solid volume fraction	ϕ_{max}	0.634	0.575
Solid volume fraction at minimum bubbling	ϕ_{mb}	0.551	0.542
Janssen's coefficient	j	0.20	0.63
Positive parameter	a	1.00	1.00
Positive parameter	b	1.00	1.00
Positive parameter (N/m^2)	c	32.00	35.00

Table 3
Experimental and theoretical values of minimum fluidization velocities.

	Powder 1		Powder 2	
	Minimum fluidization velocity (cm/s)			
D (cm)	Experimental	Theoretical	Experimental	Theoretical
10.0	0.102	0.106	0.610	0.614
5.0	0.112	0.110	0.641	0.623
2.5	0.121	0.117	0.648	0.637

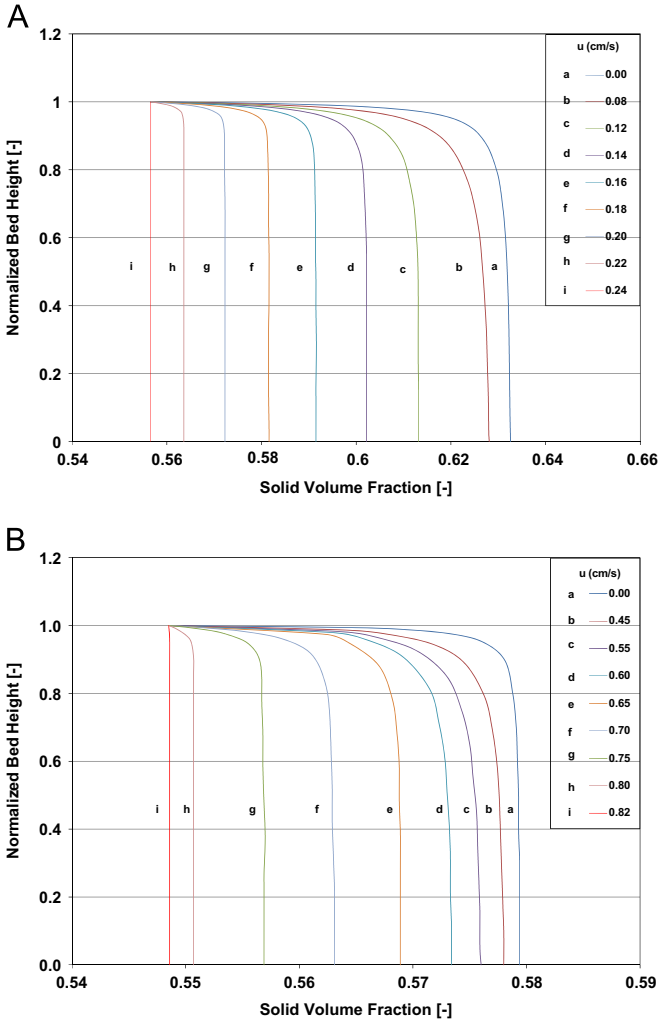

Fig. 5. Normalized bed height H/H_0 against solid volume fraction ϕ obtained theoretically. H_0 is the initial bed height. Figures A and B refer to Powders 1 and 2, respectively.

near the top of the bed, remaining fairly constant at lower heights; this shows that the bed bulk density builds up with depth. The figure also shows that the solid volume fraction at the bottom of the bed decreases as the superficial velocity of the gas increases. This is because at larger velocities the bed is more expanded, and we do expect lower and lower values of the solid volume fraction as the bed becomes progressively less packed; this indicates that as the gas velocity increases a larger fraction of the bed weight is supported by the fluid. The profiles of solid volume fraction show that the beds are not fully fluidized until the fluid velocity reaches the value of 0.24 cm/s for Powder 1 and 0.82 cm/s for Powder 2 (these velocity values are those required by the drag force to balance the effective weight of the bed when the solid volume fraction is spatially uniform and equal to $\phi_{\min}$). At such velocity values, the beds enter the fluid-like regime, becoming fully fluidized; we can tell because the solid volume fraction becomes constant over the entire depth of the bed; this implies that the particles are uniformly suspended in the fluid and that particle–particle contacts are absent. In this condition, the normal stress gradient vanishes, so that the beds can no longer transmit stress via a network of particle–particle contacts; accordingly, spatial variations in solid volume fraction no longer exist.

To see if wall friction affects the solid volume fraction profile in the bed, we ran simulations at various values of the bed diameter, keeping the superficial velocity of the fluid constant. Fig. 6 shows the plot of normalized bed height against solid volume fraction for Powders 1 and 2. We observe that, at a given value of the superficial fluid velocity, the solid volume fraction, in particular at the bottom of the bed, decreases as the value of *D* decreases. This is due to the additional support provided by the walls of the vessel, the latter reducing the component of the particle weight balanced by the action of the distributor plate. At larger velocity, the difference among the solid volume fraction profiles becomes less significant; the profiles at 0.15 cm/s for Powder 1 and 0.80 cm/s for Powder 2 are closer than those obtained at lower velocities. The reason for this is that at a high superficial gas velocity, the bed expands more, the enduring contacts among the particles reduce, and therefore the

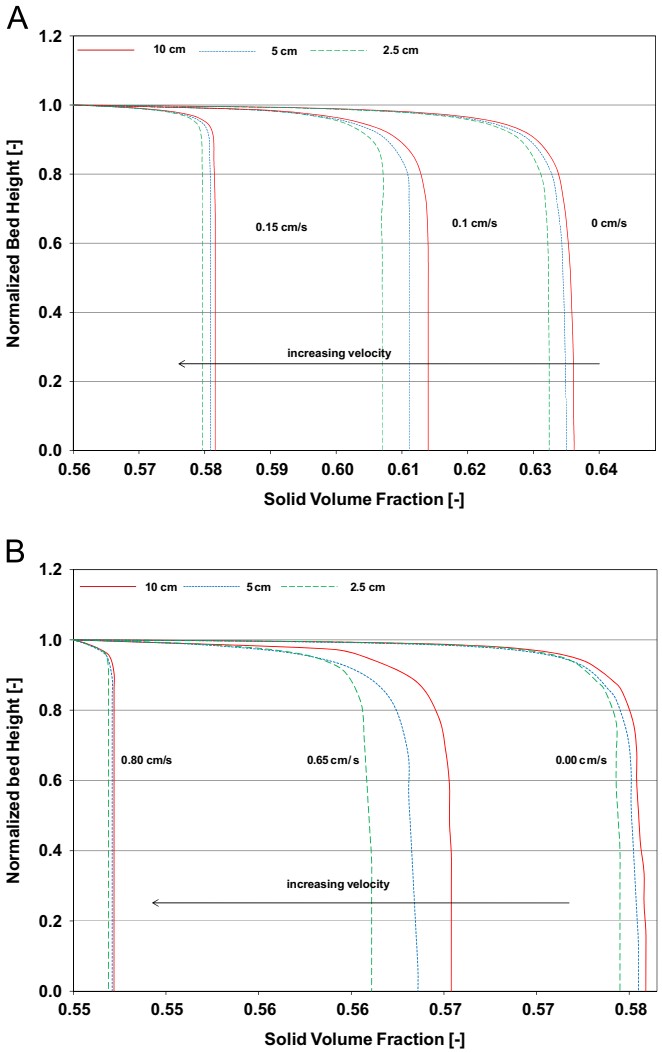

Fig. 6. Normalized bed height H/H_0 against solid volume fraction ϕ obtained theoretically for tubes of different diameter. H_0 is the initial bed height. Figures A and B refer to Powders 1 and 2, respectively.

normal stress decreases considerably. This causes a corresponding decrease in the frictional force at the walls, since the latter is directly related to the normal stress σ (refer to the second term on the left-hand side of Eq. (6)). At these high velocities, the dependence of the frictional force on the normal stress outweighs that on the vessel diameter; hence, the solid volume fraction profiles do not vary appreciably as D changes.

We did not measure experimentally the solid volume fraction profile along the bed at different superficial gas velocities, and therefore we could not directly validate the results of the model shown in Fig. 5. The validation that we carried out was indirect. As we will describe in the next section, we used the profiles to determine the parameters n^* and u_t^* present in the Richardson and Zaki (1954) correlation, which we also measured experimentally. The validation, therefore, was done in terms of these parameters.

6.2. Richardson & Zaki equation and homogeneous expansion in gas-fluidized beds

Before advancing further, let us briefly recap the aim of this work. We pointed out, in Section 2, that the correlation of Richardson and Zaki (1954) holds for both liquid-fluidized and gas-fluidized beds, but for the latter the values of the parameters n and u_t appearing in the correlation are greater than those predicted by the relations reported in the literature, which instead are reasonably accurate for liquid-fluidized beds. As said, we denote the larger values holding for gas-fluidized beds as n^* and u_t^*. These values reflect the effects of both fluid dynamic and interparticle forces, whilst the values of n and u_t reflect only the effects of the former, insofar as in liquid-fluidized beds the interparticle forces play a negligible role. We believe that the larger values of n^* and u_t^* are caused by the enduring contacts among the particles, which in turn are a manifestation of cohesiveness. In homogeneous fluidized beds in the fluid-like regime these contacts are absent, and the Richardson and Zaki parameters take on the expected fluid dynamic values denoted as n and u_t. In most of the stable interval of homogeneous expansion, nevertheless, gas-fluidized beds find themselves in the solid-like regime, where enduring contacts among particles are present. We believe that these play a key role, their presence explaining why the values of the Richardson and Zaki parameters are larger than expected. We are now in a position to put this claim to the test. The model results provide, for any given superficial gas velocity, the axial profile of the solid volume fraction, and therefore of the void fraction as well. Using these profiles, we may determine the mean values of the void fraction through the bed as a function of the superficial gas velocity; these values are those that one measures in experiments on homogeneous fluidized beds and uses in the Richardson and Zaki correlation.

To determine the n^* and u_t^* values theoretically, we operate as follows: from the profiles of solid volume fraction, we calculate the mean solid volume fraction $\overline{\phi}$ at each fluidizing velocity u in the stable interval of expansion, using the following relationship

$$\overline{\phi} = \frac{1}{H}\int_0^H \phi(z)dz \tag{17}$$

By plotting u against $\overline{\phi}$ in the Richardson and Zaki form

$$log\ u = log\ u_t^* + n^* log(1-\overline{\phi}) \tag{18}$$

we then obtain the theoretical values of n^* and u_t^* from the slope and intercept on the velocity axis of the function above, respectively. The logarithmic plot of u against $(1-\overline{\phi})$ for Powder 1 is shown in Fig. 7 for the bed with 10 cm diameter. Table 4 reports the theoretical and experimental values of n^* and u_t^* in beds of different diameters for Powders 1 and 2. The theoretical values of n^* and u_t^* obtained from our simulations show a reasonable agreement with the experimental results. In particular, the values of n^* are higher than the limiting values ascribed to n in the limit of viscous regime (discussed in Section 2). We also observe from Table 4 that the values of n^* and u_t^* increase as the bed diameter decreases; this is true for both powders and due to wall effects becoming more pronounced as the bed diameter reduces.

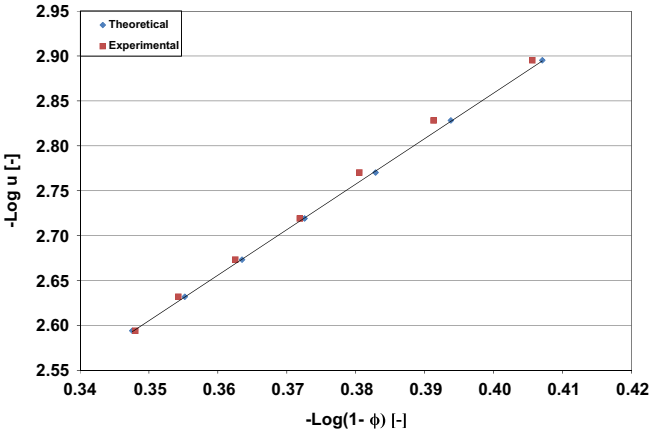

Fig. 7. Logarithmic plot of superficial gas velocity against bed voidage derived theoretically. The points represent the theoretical data, while the solid line is the linear fit.

Table 4
Summary of Richardson and Zaki (1954) parameters.

	Experimental		Theoretical		Hydrodynamic	
Powder 1						
***D* (cm)**	n^*	$u_t^*(m/s)$	n^*	$u_t^*(m/s)$	n	$u_t(m/s)$
10.0	5.36	0.183	5.04	0.144	4.6	0.10
5.0	5.96	0.309	5.49	0.204	4.6	0.10
2.5	6.62	0.587	6.35	0.437	4.6	0.10
Powder 2						
***D* (cm)**	n^*	$u_t^*(m/s)$	n^*	$u_t^*(m/s)$	n	$u_t(m/s)$
10.0	5.03	0.437	4.94	0.417	4.3	0.25
5.0	5.21	0.524	5.11	0.476	4.3	0.25
2.5	6.21	1.156	6.13	1.081	4.3	0.25

To investigate the role of enduring particle contacts in homogeneous fluidization, we reasoned as follows: if truly there were no particle–particle contacts in the fluidized bed, the particles floating freely in the fluid and the homogeneous expansion being dictated solely by fluid dynamic forces, as some authors argue, we would expect the values of n^* to be the same as the values used in our simulations to model the drag force (that is, the values of n). To explain this, let us consider Eq. (6). The latter reduces to the Richardson and Zaki equation if we neglect the contribution of stress transmitted by enduring particle contacts. In this case, the equation merely expresses the fluid dynamic force balance (where the drag force on the particles balances their effective weight) which one would expect if the bed were to be uniformly fluidized; hence, the equation yields the hydrodynamic n and u_t values used as input in the model. However, as seen from the experiments, the values of n^* and u_t^* obtained for Powders 1 and 2 are larger than the hydrodynamic ones (see Table 4). This reveals that by accounting for the stress transmitted via contacts among particles, we are able to capture the expansion profiles in the bed and to correctly predict the expansion parameters featuring in the Richardson and Zaki equation.

7. Conclusions

We adopted a one-dimensional model to investigate the behavior of gas-fluidized beds of fine particles in the homogeneous fluidization regime, accounting for enduring contacts among particles. These contacts, which are a manifestation of cohesiveness, strongly affect the expansion profiles of the beds. In particular, the values of the expansion parameters n and u_t of the Richardson and Zaki (1954) equation obtained when we accounted for stress transmitted through enduring particle contacts are higher than those obtained from purely fluid dynamic considerations. This agrees with what occurs in reality. We validated our numerical results by carrying out fluidization and defluidization experiments. The results indicate that fluid dynamic correlations for calculating the values of n and u_t, like those reported, for instance, in Gibilaro (2001), are unsuitable for describing the expansion profiles of gas-fluidized beds.

References

Batchelor, G.K., 1988. A new theory of instability of a uniform fluidized bed. J. Fluid Mech. 193, 75–110.

Cagnoli, B., Manga, M., 2004. Granular mass flows and Coulomb's friction in shear cell experiments: implications for geophysical flows. J. Geophys. Res. 109, F4.

Castellanos, A., 2005. The relationship between attractive interparticle forces and bulk behaviour in dry and uncharged fine powders. Advances in Physics 54, 263–376.

Donsi, G., Massimilla, L., 1973. Bubble-free expansion of gas-fluidized beds of fine particles. AIChE J. 19, 1104–1110.

Fortes, A.F., Caldas, P., Gallo, J.V., 1998. Particle aggregation and the van der Waals forces in gas-solids fluidization. Powder Technol. 98, 201–208.

Foscolo, P.U., Gibilaro, L.G., 1984. A fully predictive criterion for the transition between particulate and aggregative fluidization. Chem. Eng. Sci. 39, 1667–1675.

Garg, S.K., Pritchett, J.W., 1975. Dynamics of gas fluidized beds. J. Appl. Phys. 46, 4493–4500.

Geldart, D., Wong, A.C.Y., 1984. Fluidization of powders showing degree of cohesiveness-I. Bed expansion. Chem. Eng. Sci. 39, 1481–1488.

Geldart, D., Wong, A.C.Y., 1985. Fluidization of powders showing degrees of cohesiveness - II. Experiments on rates of de-aeration. Chem. Eng. Sci. 40, 653–661.

Geldart, D., 1973. Types of gas fluidization. Powder Technol. 7, 285–292.

Gibilaro, L.G., 2001. Fluidization-Dynamics. Butterworth Heinemann, Oxford.

Godard, K.M.S., Richardson, J.F., 1968. The behaviour of bubble-free fluidized beds. I. Chem. Eng. Symp. Ser. 30, 126.

Härtl, J., Ooi, J.Y., 2011. Numerical investigation of particle shape and particle friction on limiting bulk friction in direct shear tests and comparison with experiments. Powder Technol. 212, 231–239.

Jackson, R., 1963. The mechanics of fluidized beds: Part I. The stability of the state of uniform fluidization. Trans. Instn. Chem. Eng. 41, 13–21.

Jackson, R., 2000. The Dynamics of Fluidized Particles. Cambridge University Press, Cambridge.

Katz, H., Sears, J.T., 1969. Electric field phenomena in fluidized and fixed bed. Can. J. Chem. Eng. 47, 50–53.

Khan, A.R., Richardson, J.F., 1989. Fluid-particle interactions and flow characteristics of fluidized beds and settling suspensions of spherical particles. Chem. Eng. Commun. 78, 111.

Lettieri, P., Newton, D., Yates, J.G., 2002. Homogeneous bed expansion of FCC catalysts, influence of temperature on the parameters of the Richardson-Zaki equation. Powder Technol. 123, 221–231.

Loezos, P.N., Costamagna, P., Sundaresan, S., 2002. The role of contact stresses and wall friction on fluidization. Chem. Eng. Sci. 57, 5123–5141.

Mabrouk, R., Chaouki, J., Guy, C., 2008. Wall surface effects on particle–wall friction factor in upward gas–solid flows. Powder Technol. 186, 80–88.

Massimilla, L., Donsi, G., Zucchini, C., 1972. The structure of bubble-free gas fluidized beds of fine fluid cracking catalyst particles. Chem. Eng. Sci. 27, 2005–2015.

Mazzei, L., 2008. Eulerian Modelling and Computational Fluid Dynamics Simulation of Mono and Polydisperse Fluidized Suspensions (Ph.D. dissertation). Department of Chemical Engineering, University College London, London.

Mazzei, L., Lettieri, P., Elson, T., Colman, D., 2006. A revised monodimensional particle bed model for fluidized beds. Chem. Eng. Sci. 61, 1958–1972.

Mutsers, S.M.P., Reitema, K., 1977. The effect of inter-particle forces on the expansion of a homogeneous gas fluidized bed. Powder Technol. 18, 239–248.

Reitema, K., 1973. The effect of interparticle forces on the expansion of a homogeneous gas-fluidized bed. Chem. Eng. Sci. 28, 1493–1497.

Richardson, J.F., Zaki, W.N., 1954. Sedimentation and fluidization. Trans. Inst. Chem. Eng. 32, 35–53.

Rowe, P.N., 1987. A convenient empirical equation for estimation of the Richardson and Zaki exponent. Chem. Eng. Sci. 42, 2795.

Srivastava, A., Sundaresan, S., 2002. Role of wall friction in fluidization and standpipe flow. Powder Technol. 124, 45–54.

Tsinontides, S.C., Jackson, R., 1993. The mechanics of gas fluidized beds with an interval of stable fluidization. J. Fluid Mech. 255, 237–274.

Valverde, J.M., Ramos, A., Castellanos, A., Watson, P.K., 1998. The tensile strength of cohesive powders and its relationship to consolidation, free volume and cohesivity. Powder Technol. 97, 237–245.

Valverde, J.M., Quintanilla, M.A.S., Castellanos, A., Mills, P., 2003a. Experimental study on the dynamics of gas-fluidized beds. Phys. Rev. Lett. 67, 016303.

Valverde, J.M., Castellanos, A., Mills, P., Quintanilla, M.A.S., 2003b. Effect of particle size and interparticle force on the fluidization behavior of gas-fluidized beds. Phys. Rev. 67, 1–6 051305.

Wallis, G.B., 1969. One-Dimensional two-phase flow. McGraw-Hill.

Watson, P.K., Valverde, J.M., Castellanos, A., 2001. The tensile strength and free volume of cohesive powders compressed by gas flow. Powder Technol. 115, 45–50.